ChemPhysChem

Research Article
doi.org/10.1002/cphc.202300536

Chemistry Europe
European Chemical Societies Publishing

www.chemphyschem.org

Fe-Doped CoS_2 Nanoarrays: Efficient Electrocatalytic Nitrate Reduction to Ammonia under Ambient Conditions

Xiaoliang Lu,[a] Jinzhi Zhou,[a] Jinxiu Zhao,[a] Dan Wu,[a] Xuejing Liu,[a] Xiang Ren,*[a] Qin Wei,*[a] and Huangxian Ju[a]

The electrocatalytic nitrate reduction reaction (NO_3^-RR) enables the reduction of nitrate to ammonium ions under ambient conditions. It was considered as an alternative reaction for the production of ammonia (NH_3) in recent years. In this paper, we report that the Fe doping CoS_2 nanoarrays can effectively catalyze the formation of NH_3 from nitrate (NO_3^-) under ambient conditions. This is mainly due to the increase of the NO_3^- reaction active site by Fe doping and the porous nanostructure of the catalyst, which greatly improves the catalytic activity. Specifically, at −0.9 V vs. RHE, the NH_3 yield rate (R_{NH3}) of Fe—CoS_2/CC is 17.8×10^{-2} mmol h^{-1} cm^{-2} with Faraday Efficiency (FE) of 88.93%. Besides, such catalyst shows good durability and catalytic stability, which provides the possibility for the future application of electrocatalytic NH_3 production.

Introduction

Ammonia (NH_3) is one of the most widely produced chemicals in the world and is a basic chemical raw material for chemical production.[1–5] In addition, NH_3 is particularly important for the production of ammonium nitrate, urea and other types of nitrogen-containing compound fertilizers.[6–9] At the same time, NH_3 is an emerging energy carrier that the hydrogen content of liquid NH_3 is 17.6%, while the methanol content is only 12.5%.[6] Therefore, NH_3 may be a promising candidate for the future of the hydrogen economy.[7] Moreover, NH_3 occupies an indispensable position in future population development.[10] However, the only method currently capable of industrial NH_3 synthesis (the Haber-Bosch process) suffers from harsh conditions, high equipment requirements, high energy consumption (consuming 2% of the global energy supply each year) and low conversion rates, which are increasingly incompatible with economic and social development requirements.[11] Accordingly, finding ways to achieve high NH_3 yield rate (R_{NH3}), high current density and low energy consumption, as well as low cost and large scale production of NH_3 will be the focus of future research.[12]

In recent years, the electrocatalytic nitrate reduction reaction (NO_3^-RR) has attracted much attentions.[13–16] Compared to the conventional Haber-Bosch process, NO_3^-RR operates under mild conditions and has lower N=O bonds dissociation energy (204 kJ mol^{-1}) compared to the N≡N bonds (941 kJ mol^{-1}),[17] but NO_3^-RR requires an efficient nitrate electrocatalyst to enhance the reaction process. At the same time, the NO_3^-RR reaction would generate a series of by-products and hydrogen precipitation reactions (HER) that hinder the reaction process.[18] Therefore, efficient catalysts need to be found to speed up the reaction process. Noble metal catalysts have better catalytic effect on NO_3^-RR. However, precious metals are not only insufficient in quantity but also expensive.[19–21] Hence, it is urgent to find earth-rich catalysts to replace the precious metal catalysts.[22] In addition, nitrates (NO_3^-) in water will have a negative impact on humans and the environment, drinking water containing NO_3^- can lead to methemoglobinemia, which causes fatigue, shortness of breath, lack of oxygen to the brain and even death.[10,18] Consequently, there is a great need for efficient conversion of harmful nitrates in the environment into useful NH_3.[5]

Transition metal sulfide (TMDs) makes up for the deficiency of precious metal surface content and has good electrocatalytic performance.[23] Other than that the transition metals have unique d-orbital structures and abundant electron cloud densities, enabling efficient electrocatalytic activity.[24,25] In recent years, it has been shown that CoS_2 has attracted a lot of attention as an efficient electrocatalyst, especially in electrocatalytic nitrogen reduction (NRR) which has shown to exhibit good performance.[26] Inspired by the Fe-based catalysts in the Haber-Bosch process, a recent study proposed the use of Fe single atoms as catalysts for efficient reduction of NO_3^- to produce NH_3.[27] It can effectively reduce the coupling of N≡N bonds, increase the reaction active sites and improve the selectivity of NH_3 synthesis.[28–30] In addition, Co has important applications in electrolysis of water, NRR, etc. due to its controllable electronic structure. Furthermore Fu et al. recently developed a Co_3O_4/carbon felt (CF) electrode with a 3D structure with a high rate constant,[30] which successfully improved the kinetics of the reaction, and calculations showed that Co(II) facilitated the H* production. Wang et al. investigated the relationship between the intermediate adsorption energy and the NO_3^-RR activity of CuNi catalysts to address the problem of how to adjust the catalyst structure to improve the

[a] X. Lu, J. Zhou, J. Zhao, Prof. D. Wu, X. Liu, Prof. X. Ren, Prof. Q. Wei, Prof. H. Ju
Key Laboratory of Interfacial Reaction & Sensing Analysis in Universities of Shandong
School of Chemistry and Chemical Engineering, University of Jinan
250022 Jinan, Shandong (China)
E-mail: chem_renx@163.com
sdjndxwq@163.com

Supporting information for this article is available on the WWW under https://doi.org/10.1002/cphc.202300536

catalytic activity.[31] Liu et al. revealed selective tunability for nitrite and ammonia based on the high NO_3^- to NO_2^- selectivity and NO_3^- to N_2 conversion of OD–Ag.[32] In this work, we propose a Fe–CoS_2/CC catalyst with excellent electrocatalytic activity as an electrode material using doping modulation. It is able to reduce the reaction activation energy and therefore accelerate the reaction process. CoS_2 promotes H* production as well as reduces by-product generation, thus improving selectivity, while Fe incorporation effectively increases the active site for the NO_3^- reaction.[33,34] In addition, the catalyst has a porous nanosheet structure, and the large specific surface area can also enhance the catalytic efficiency.[35] In a mixture of 0.1 M Na_2SO_4 and 0.1 M $NaNO_3$, the NH_3 yield rate (R_{NH3}) of Fe–CoS_2/CC is 17.8×10^{-2} mmol h^{-1} cm^{-2} with Faraday efficiency (FE) of 88.93%, and it exhibits good durability and catalytic stability.

Results and Discussion

The composition and crystal structure of Fe–CoS_2/CC were investigated by X-ray diffraction (XRD) technique. In Figure 1a, the five diffraction peaks near 32.3°, 36.2°, 39.8°, 46.3°, and 54.9° correspond to the five diffraction surfaces (200), (210), (211), (220), and (311) in typical CoS_2 (JCPDS No. 41-1471), and the typical diffraction peaks of Fe are not found. Comparison with the reference spectra of pure CoS_2 shows that there is a slight peak shift in the XRD spectrum after Fe doping, it indicating that the Fe doping does not change the crystalline structure of the CoS_2 matrix and the offset may be an effect of the different ionic radii of Fe doping and Co. The scanning electron microscopy (SEM) images (Figure 1b) show that the nanosheets on the carbon cloth (CC) surface are closely arranged and uniformly distributed. Besides, the transmission electron microscope (TEM) image (Figure 1c) demonstrates the porous nanosheet structure of the material.

The lattice stripes with an interval of 2.76 Å can be found in the high-resolution TEM (HRTEM) shown in Figure 1d, corresponding to the (200) crystal plane of CoS_2. The corresponding energy dispersive X-ray (EDS) elemental mapping (Figure 1e) clearly shows the total elemental spectra of Fe–CoS_2/CC and the uniform distribution of S, Co and Fe elements, and it also demonstrates the successful preparation of Fe-doped CoS_2. The corresponding selected area electron diffraction (SAED) (Figure 1f) presents crystalline surfaces that are consistent with the XRD test results of CoS_2.

The elemental composition and valence states of Fe–CoS_2/CC were characterized. The total spectrum of X-ray photoelectron spectroscopy (XPS) is shown in Figure 2a. Once again, it is further proved that Fe, Co and S elements exist in the product. Besides, Figure 2b illustrates 2p spectrum of the Fe, the binding energy peaks (BEs) at 713.9 eV and 711.0 eV correspond to Fe $2p_{3/2}$, and the BEs at 720.55 eV corresponds to Fe $2p_{1/2}$.[36] The Co 2p spectrum (Figure 2c) shows that the Co $2p_{3/2}$ region corresponds to the two BEs at 776.42 eV and 780.08 eV. The Co $2p_{1/2}$ region corresponds to two BEs at 791.45 eV and 796.14 eV,[37,38] which were accompanied by an

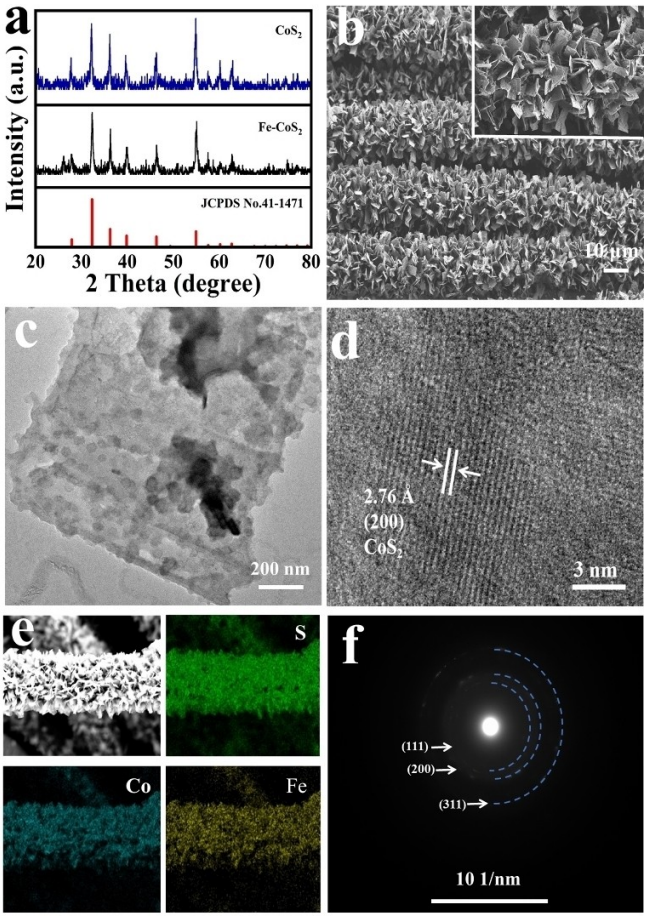

Figure 1. (a) XRD patterns of CoS_2/CC and Fe–CoS_2/CC. (b) SEM images of Fe–CoS_2/CC. (c) TEM and (d) HRTEM images of Fe–CoS_2/CC. (e) EDX mapping of S, Co, and Fe for Fe–CoS_2/CC. (f) SAED image taken from Fe–CoS_2/CC.

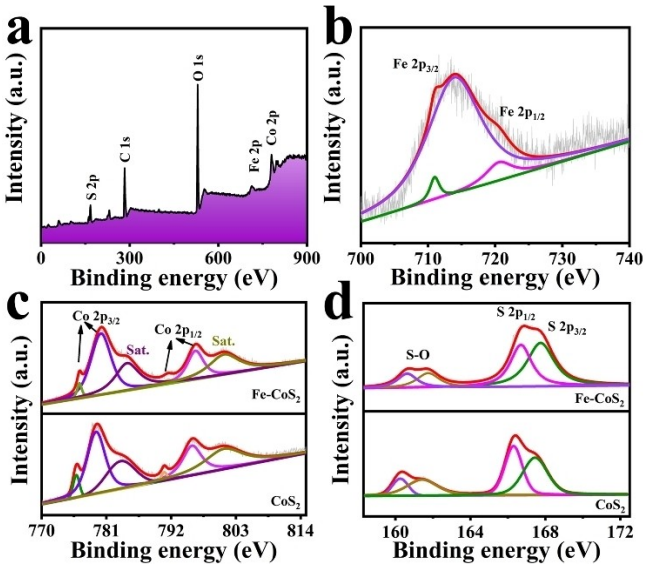

Figure 2. (a) Total XPS spectrum of Fe–CoS_2/CC. (b) XPS spectra of Fe 2p in Fe–CoS_2/CC. (c) XPS spectra of Co 2p in Fe–CoS_2/CC. (d) XPS spectra of S 2p in Fe–CoS_2/CC.

oscillating satellite peak, consistent with the reported Co(II) in the literature and the BEs at the peak position was negatively shifted compared with that of pure CoS_2. The spectra of S 2p shows two distinct peaks in Figure 2d, S $2p_{1/2}$ and S $2p_{3/2}$ appearing at two positions with BEs of 166.7 eV and 167.75 eV, and S–O peaks were also found at BEs of 160.63 eV and 161.75 eV, indicating the possible presence of oxides in Fe–CoS_2/CC. In addition, the BEs of the exiting peak positions were all positively shifted compared to those of pure CoS_2. Due to the change in BEs at the position of the exiting peak, it is suggested that there may be strong electronic interactions after Fe doping, which is important for regulating the electronic environment and thus for electrocatalytic nitrate reduction.

Preliminary evaluation of Fe–CoS_2/CC performance by the linear sweep voltammetry (LSV) test. Figure 3a shows the LSV curves of Fe–CoS_2/CC in electrolyte solution containing NO_3^- and pure Na_2SO_4 electrolyte solution. It can be seen that start at the inflection point the curve with NO_3^- has higher current density and lower voltage, which demonstrate that Fe–CoS_2/CC catalyzed the reduction of NO_3^-. Further by ten LCV tests (Figure 3b), Fe–CoS_2/CC was found to have stable catalytic performance. In addition, we selected five potentials between −0.7 V vs. RHE and −1.1 V vs. RHE for testing, and the current density versus time curves are shown in Figure 3c. The current density increases with the potential and tends to be stable during the test. The required test calibration curves (Figure S1–S3) show a good linear relationship. The cathodic electrolyte obtained from the test was diluted to a suitable concentration for color development, and the absorbance was measured by UV-Vis spectrophotometer, and the absorbance curves for each potential were plotted as shown in Figure 3d. It can be seen that the highest absorbance was measured at −0.9 V vs. RHE. At the same time, the electrolyte was tested for by-products after 1 h of electrolysis, and the UV-Vis absorption spectra of NO_3^- and NO_2^- were used to make a preliminary determination of their concentrations (Figure S4), and it was clear that there was not much NO_3^- and NO_2^- left in the tested electrolyte, fully indicating the adequate conversion of NO_3^- to NH_4^+.

Finally, the measured absorbance was substituted into the standard working curve to calculate the concentration. The R_{NH3} and FE calculated according to equation are shown in Figure 4a. The remaining nitrate content was also assayed and its conversion is given in Figure 4b. From this we conclude that in an electrolyte solution containing 0.01 M NO_3^-, the FE was as high as 88.93% at −0.9 V vs. RHE with an R_{NH3} of 17.8×10^{-2} mmol h^{-1} cm^{-2}, which is superior to most of the reported catalysts. Table S1 shows the performance of Fe–CoS_2/CC compared with other catalysts. In addition, we also compared the FE obtained from the generation of NH_3 by Fe–CoS_2/CC at a given potential test with the by-product NO_2^- (Figure 4c). The results showed that only trace amounts of NO_2^- were detected and the FE at all potentials did not exceed 0.3%, which demonstrating that the reaction generates NO_2^- and then proceeded to the latter protonation process, and also reflected the excellent selectivity of Fe–CoS_2/CC. Further, we did control experiments to verify the source of NH_3. As shown in Figure 4d, the experiments verified that NH_3 was produced by NO_3^-RR on Fe–CoS_2/CC, and the NH_3 yield was only 0.40×10^{-2} mmol h^{-1} cm^{-2} in the open circuit (OPC) state, and negligible in PBS (0.32×10^{-2} mmol h^{-1} cm^{-2}) and fresh electrolyte (0.36×10^{-2} mmol h^{-1} cm^{-2}). Therefore, the effects from experimental reagents and equipment were excluded.

The electrochemical performance of Fe–CoS_2/CC was verified again by designing comparative experiments. We obtained Fe/CC, Fe–CoS_2/CC and CoS_2/CC for electrocatalytic tests at −0.9 V vs. RHE, respectively, and obtained UV-Vis is absorption spectra as shown in Figure 5a. The corresponding R_{NH3} and FEs are shown in Figure 5b. The results show that the R_{NH3} and FE of Fe–CoS_2/CC are much higher than those of the other two catalysts, which proved that the Fe doping mentioned an enhanced effect on the catalytic activity of CoS_2. To our

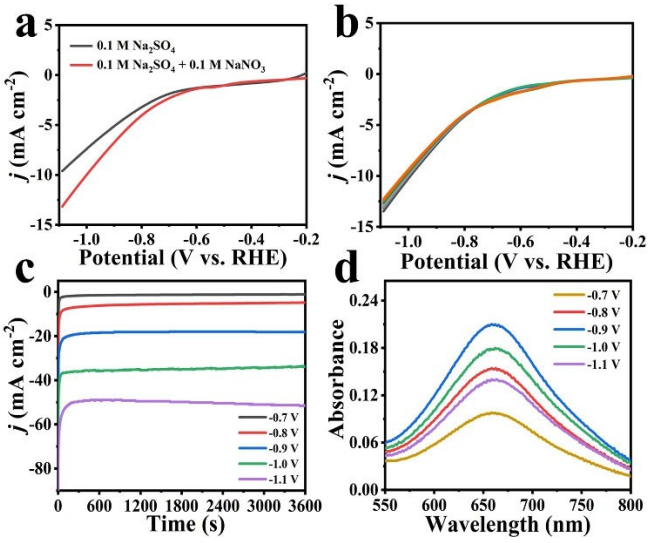

Figure 3. (a) LSV curves of Fe–CoS_2/CC under electrolyte solutions containing NO_3^- and without NO_3^-, respectively. (b) Ten LSV curves of Fe–CoS_2/CC under an electrolyte solution containing NO_3^-. (c) Current density versus time curves for Fe–CoS_2/CC at five potentials. (d) UV-Vis absorption spectra of Fe–CoS_2/CC at five potentials.

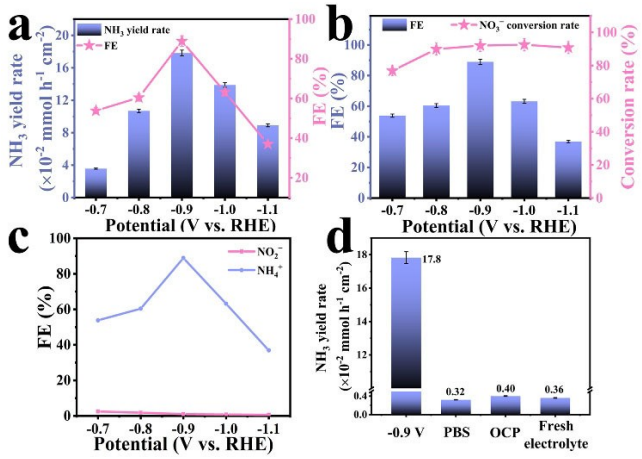

Figure 4. (a) R_{NH3} and FEs of Fe–CoS_2/CC at five potentials. (b) Conversion rates of NO_2^- and FEs of NH_4^+ for Fe–CoS_2/CC at five potentials. (c) FEs of Fe–CoS_2/CC in the generation of NH_3 and NO_2^- at five potentials (d) NH_3 yields of Fe–CoS_2/CC for the NO_3^-RR at different conditions.

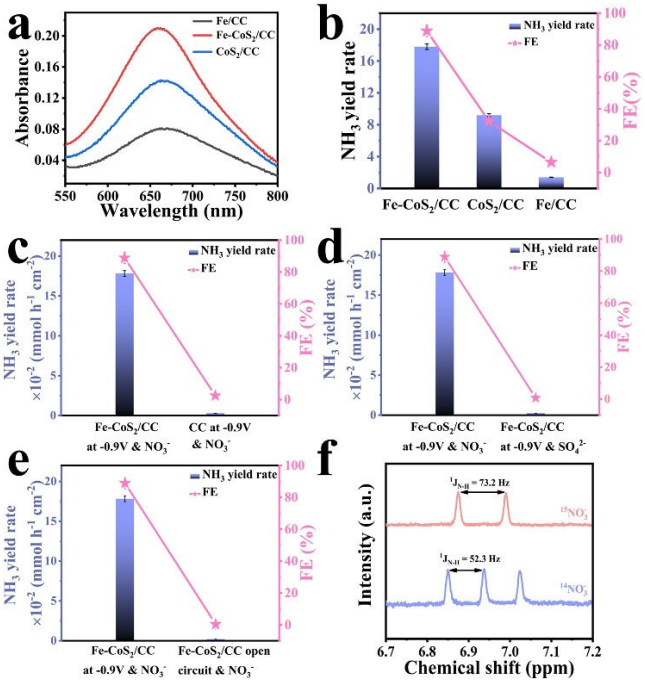

Figure 5. (a) UV-Vis absorption spectra of Fe/CC, Fe–CoS_2/CC and CoS_2/CC after color development. (b) R_{NH3} and FE at −0.9 V vs. RHE for Fe/CC, Fe–CoS_2/CC and CoS_2/CC. (c) R_{NH3} and FE of control experiments (1), (2). (d) R_{NH3} and FE of control experiments (1), (3). (e) R_{NH3} and FE of control experiments (1), (4). (f) ^1H NMR spectra of $^{14}NH_4^+$ and $^{15}NH_4^+$ after NO_3^-RR tests.

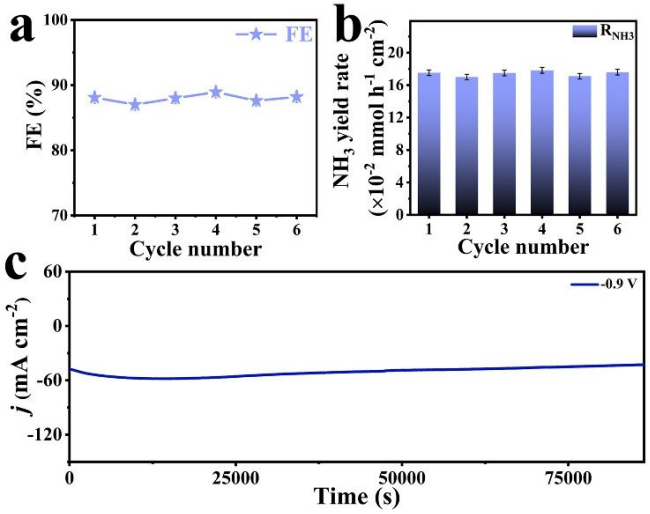

Figure 6. (a) Average R_{NH3} obtained from six replicate experiments of Fe–CoS_2/CC at −0.9 V vs. RHE. (b) Average FE obtained from six replicate experiments of Fe–CoS_2/CC at −0.9 V vs. RHE. (c) Current density versus time curve for Fe–CoS_2/CC after 10 hours of continuous testing at −0.9 V vs. RHE.

surprised, Fe/CC alone also had some catalytic effect on nitrate reduction. To demonstrate the issue of the source of NH_3 production, four sets of controlled experiments were designed: (1) Catalyst: Fe–CoS_2/CC, electrolyte solution: a mixture of 0.1 M Na_2SO_4 and 0.1 M $NaNO_3$, potential: −0.9 V vs. RHE. (2) Catalyst: bare carbon cloth, electrolyte solution: a mixture of 0.1 M Na_2SO_4 and 0.1 M $NaNO_3$, potential: −0.9 V vs. RHE. (3) Catalyst: Fe–CoS_2/CC, electrolyte solution: 0.1 M Na_2SO_4 solution, potential: −0.9 V vs. RHE. (4) Catalyst: Fe–CoS_2/CC, electrolyte solution: a mixture of 0.1 M Na_2SO_4 and 0.1 M $NaNO_3$, potential: open circuit. The results, as illustrated in Figure 5c, d, e, show that almost no NH_3 was produced in the control experiments (2) (3) (4), which can tentatively indicate that the NH_3 produced originated from the reduction of NO_3^- in solution. For accurate verification, we also performed ^1H nuclear magnetic resonance (NMR) spectroscopy on the tested solution. And the results, as shown in Figure 5d, showed that the hydrogen NMR spectra (600 MHz) of electrolytes with $^{15}NO_3^-$ and $^{14}NO_3^-$ as reactants show different typical peaks. The former shows typical double peaks of $^{15}NH_4^+$, while the latter shows typical triple peaks of $^{14}NH_4^+$, which was able to demonstrate that the NH_3 produced was exclusively from nitrate in the electrolyte solution. The electrochemically active surface area (ECSA) based on the double-layer capacitance (Cdl) can also reveal that active sites are more efficient for Fe–CoS_2/CC (Figure S6). Moreover, we estimated the charge transfer resistance of both catalysts by electrochemical impedance (EIS) (Figure S7), and Fe–CoS_2/CC showed a smaller Nyquist semicircle radius, which is more favorable for charge transfer during catalysis, fully demonstrating that Fe doping is beneficial to improve the electrochemical properties. We performed several reproducibility tests (Figure 6(a) and (b)) and found that the obtained R_{NH3} and FEs varied with little fluctuation, demonstrating the good reproducibility of the catalyst. In addition, a good catalyst must not only have high catalytic activity, but also ensure catalytic stability and durability. We conducted a performance test of Fe–CoS_2/CC at −0.9 V vs. RHE for 10 h. The obtained current density versus time curves are shown in Figure 6(c) demonstrating that our prepared catalysts can catalyze stably for at least 10 h. In addition, XRD (Figure S4(a)) and SEM images (Figure S5(b)) after long time electrolysis show that the Fe–CoS_2/CC crystallographic parameters and material surface are almost unchanged, which further proves the good stability and durability of Fe–CoS_2/CC. Further, TEM (Figure S4(c)) and HRTEM (Figure S4(d)) after long time electrolysis showed that the Fe–CoS_2/CC lattice structure did not change, and the stability of the material was also verified.

Conclusions

Overall, the as-prepared Fe–CoS_2/CC porous catalyst can achieve high R_{NH3} (17.8×10^{-2} mmol h^{-1} cm^{-2}) and FE (88.93%), demonstrating the catalytic activity promotion of CoS_2 was drived by Fe doping. In addition, the catalyst has strong selectivity and durability. The results open a new pathway for the selective reduction of nitrate to ammonia under benign conditions.[39–41]

Experimental Section

Preparation of Fe–CoS_2/CC and CoS_2/CC

Firstly, $Co(NO_3)_2 \cdot 6H_2O$ (0.5821) g, $Fe(NO_3)_3 \cdot 9H_2O$ (0.0808 g) and $CO(NH_2)_2$ (0.6006 g) were dissolved in 60.0 mL deionized water, After 30 minutes of continuous stirring, the solution was transferred to a 50.0 mL stainless steel reactor lined with PTFE. The treated carbon cloth (2×3 cm) was placed, and then the autoclave was sealed and reacted at 120 °C for 12 h. After the reaction kettle cooled to room temperature, the carbon cloth specimens were removed, washed thoroughly with deionized water and ethanol alternately for several times, dried at 60 °C for 6 h, and taken out and set aside. Next, CH_3CSNH_2 (0.1800 g) was dissolved in 50.0 mL of anhydrous ethanol, mixed and transferred to a PTFE-lined reaction vessel, The resulting precursor carbon cloth was added and reacted at 180 °C for 12 h. After the reaction kettle was cooled to room temperature, the carbon cloth specimens were removed, washed thoroughly with anhydrous ethanol several times, and dried at 60 °C for 6 h to obtain Fe–CoS_2/CC. Under the same conditions, pure CoS_2/CC was prepared without the addition of Fe.

Electrochemical Measurements

Electrocatalytic nitrate reduction experiments were performed in an H-type electrolytic cell separated by a proton exchange membrane. Prior to the electrocatalytic nitrogen reduction reaction test, the proton exchange membranes were pretreated with 5% H_2O_2 sonication for 20 min followed by heating with ultrapure water at 80 °C for 8 h. The electrolyte is a mixture of 0.1 mol L^{-1} Na_2SO_4 and 0.01 mol L^{-1} $NaNO_3$. The reaction process was measured electrochemically using a CHI760D electrochemical workstation in a standard three-electrode system with the catalyst Fe–CoS_2/CC as the working electrode, Ag/AgCl as the reference electrode, and graphite rod as the counter electrode. Argon gas is passed to the cathode for half an hour before the test to exclude environmental interference, and the test time is 1 h. After the test, the solution in the cathode cell of the electrolytic cell is collected and used for subsequent tests. All experiments were conducted under ambient conditions.

Determination of NH_3

NH_3 produced by indophenol blue method was determined by ultraviolet absorption spectrometry. Among them, 4.0 mL post-test solution was obtained from the cathode of the electrolytic cell. Then 50.0 μL oxidant (0.4 M $C_7H_5O_3Na$ + 0.32 M NaOH), 500.0 μL colorant (NaClO + 0.75 M NaOH) and 50.0 μL catalyst ($C_5FeN_6Na_2O$, 1 wt%) were added. UV-Vs is absorption spectrum were measured after standing at 25 °C for 1 hour in the dark. The concentration of indophenol blue was determined by absorbance at 660 nm. The concentration-absorbance curves were calibrated using a series of standard ammonium chloride solutions. After three independent calibrations, the fitting curve ($Y = 0.462X + 0.069$, $R^2 = 0.999$) showed a good linear relationship between absorbance value and NH_4Cl concentration.

Determination of NO_2^-

Color developer: add p-aminobenzenesulfonamide (4.0000 g), N-(1-naphthyl) ethylenediamine salt (0.2000 g), phosphoric acid (10.0 mL) to 50.0 mL of water, dissolve and mix well, then store at low temperature and avoid light. Take 5.0 mL of electrolyte from the cathode of the electrolytic cell, add 0.1 mL of color developer, mix well, let it stand and avoid light for 20 min, test the absorbance at 540 nm with UV-Vis spectrophotometer, and draw the standard working curve of concentration-absorbance. The final working curve was $Y = 1.311X + 0.016$, $R^2 = 0.999$ with good linearity.

Determination of NO_3^-

Color rendering agent: hydrochloric acid (1 mol L^{-1}), sulfamic acid (0.8 wt%). The cathode cell electrolyte was diluted to a suitable concentration, and 5.0 mL was added with 0.1 mL hydrochloric acid (1 mol L^{-1}) and 0.01 mL sulfamic acid (0.8 wt%), mixed well, and left to develop color for 15 min, and the absorbance at 220 nm and 275 nm was measured by UV-Vis spectrophotometer, and $A = A_{220nm} - 2\,A_{275nm}$, and the concentration-absorbance was plotted. The final working curve was $Y = 0.105X - 0.015$, $R^2 = 0.998$ with good linearity.

Calculation of the Performance Parameters

NH_3 formation was calculated as follows:

$$NH_3 \text{ formation rate} = [NH_4^+] \times V/(17 \times t \times A)\ (\text{mol s}^{-1}\,\text{cm}^{-2}) \quad \text{(Equation S1)}$$

The FE was calculated according to following equation:

$$FE = 8 \times F \times [NH_4^+] \times V/(17 \times Q) \quad \text{(Equation S2)}$$

The NO_2^- FE was calculated according to following equation:

$$FE = 2 \times F \times [NO_2^-] \times V/(46 \times Q) \quad \text{(Equation S3)}$$

The NO_3^- FE was calculated according to following equation:

$$NO_3^- \text{ conversion} = \Delta C_{NO3-}/C_0 \quad \text{(Equation S4)}$$

where $[NH_4^+]$ is the concentration of NH_4^+ (μg/mL) obtained from the standard working curve; V is the volume of the cathodic reaction cell solution (mL); t is the time of electrolysis reaction (h); A is the area of the loaded catalyst carbon cloth (cm^2); F is the Faraday constant (c/mol); Q is the measured power (C); $[NO_2^-]$ is the NO_2^- concentration (μg/mL) obtained from the standard working curve of the by-product; C0 is the initial concentration of NO_3^- in the electrolyte solution; ΔC_{NO3-} the difference in concentration of the electrolyte solution after catalytic concentration difference before and after reduction.

Supporting Information

Additional references cited within the Supporting Information.[42–48]

Acknowledgements

This study was supported by the National Natural Science Foundation of China (No. 22204059), the Natural Science Foundation of Shandong Province (No. ZR2021QB120, ZR2022QB021), the Foundation of Yunnan Key Laboratory of Rural Energy Engineering (Yunnan Normal University), the

Special Foundation for Taishan Scholar Professorship of Shandong Province (Prof. Q. Wei).

Conflict of Interests

The authors declare no conflict of interest.

Data Availability Statement

The data that support the findings of this study are available from the corresponding author upon reasonable request.

Keywords: doping engineering · electrocatalysis · faraday efficiency · nanosheet arrays · nitrate reduction.

[1] A. T. Wijayanta, T. Oda, C. W. Purnomo, T. Kashiwagi, M. Aziz, *Int. J. Hydrogen Energy* **2019**, *44*, 15026–15044.
[2] X. Ren, J. Zhao, Q. Wei, Y. Ma, H. Guo, Q. Liu, Y. Wang, G. Cui, A. M. Asiri, B. Li, B. Tang, X. Sun, *ACS Cent. Sci.* **2019**, *5*, 116–121.
[3] Y. Kojima, M. Yamaguchi, *Int. J. Hydrogen Energy* **2020**, *45*, 10233–10246.
[4] A. Klerke, C. H. Christensen, J. K. Nørskov, T. Vegge, *J. Mater. Chem. A.* **2008**, *18*, 2304–2310.
[5] W. Guo, K. Zhang, Z. Liang, R. Zou, Q. Xu, *Chem. Soc. Rev.* **2019**, *48*, 5658–5716.
[6] J. Guo, P. Chen, *Chem.* **2017**, *3*, 709–712.
[7] X. Zhu, S. Mou, Q. Peng, Q. Liu, Y. Luo, G. Chen, S. Gao, X. Sun, *J. Mater. Chem. A.* **2020**, *8*, 1545–1556.
[8] Q. Wu, Q. Gao, L. Sun, H. Guo, X. Tai, D. Li, L. Liu, C. Ling, X. Sun, *Chin. J. Catal.* **2021**, *42*, 482–489.
[9] J. Wang, L. Yu, L. Hu, G. Chen, H. Xin, X. Feng, *Nat. Commun.* **2018**, *9*, 1795.
[10] M. Duca, M. T. M. Koper, *Energy Environ. Sci.* **2012**, *5*, 9726–9742.
[11] H. Liu, P. Wu, H. Li, Z. Chen, L. Wang, X. Zeng, Y. Zhu, Y. Jiang, X. Liao, B. S. Haynes, J. Ye, C. Stampfl, J. Huang, *Appl. Catal. B.* **2019**, *259*,118026.
[12] C. Guo, J. Ran, A. Vasileff, S.-Z. Qiao, *Energy Environ. Sci.* **2018**, *11*, 45–56.
[13] Y. Wang, W. Zhou, R. Jia, Y. Yu, B. Zhang, *Angew. Chem. Int. Ed.* **2020**, *59*, 5350–5354.
[14] Z. Li, J. Liang, Q. Liu, L. Xie, L. Zhang, Y. Ren, L. Yue, N. Li, B. Tang, A. A. Alshehri, M. S. Hamdy, Y. Luo, Q. Kong, X. Sun, *Mater. Today.* **2022**, *23*,100619.
[15] R. Jia, Y. Wang, C. Wang, Y. Ling, Y. Yu, B. Zhang, *ACS Catal.* **2020**, *10*, 3533–3540.
[16] Z. Li, G. Wen, J. Liang, T. Li, Y. Luo, Q. Kong, X. Shi, A. M. Asiri, Q. Liu, X. Sun, *Chem. Commun. (Camb.)* **2021**, *57*, 9720–9723.
[17] E. D. Glendening, A. M. Halpern, *J. Chem. Phys.* **2007**, *127*, 164307.
[18] S. Garcia-Segura, M. Lanzarini-Lopes, K. Hristovski, P. Westerhoff, *Appl. Catal. B.* **2018**, *236*, 546–568.
[19] J. Lim, C.-Y. Liu, J. Park, Y.-H. Liu, T. P. Senftle, S. W. Lee, M. C. Hatzell, *ACS Catal.* **2021**, *11*, 7568–7577.
[20] M. Nazemi, S. R. Panikkanvalappil, M. A. El-Sayed, *Nano Energy.* **2018**, *49*, 316–323.
[21] Y. Han, X. Zhang, W. Cai, H. Zhao, Y. Zhang, Y. Sun, Z. Hu, S. Li, J. Lai, L. Wang, *J. Colloid Interface Sci.* **2021**, *600*, 620–628.
[22] Q. Liu, T. Xu, Y. Luo, Q. Kong, T. Li, S. Lu, A. A. Alshehri, K. A. Alzahrani, X. Sun, *Curr. Opin. Electrochem.* **2021**, *29*,100766.
[23] F. Song, L. Bai, A. Moysiadou, S. Lee, C. Hu, L. Liardet, X. Hu, *J. Am. Chem. Soc.* **2018**, *140*, 7748–7759.
[24] L. Zhang, L. X. Ding, G. F. Chen, X. Yang, H. Wang, *Angew. Chem. Int. Ed.* **2019**, *58*, 2612–2616.
[25] S. Yang, W. Ye, D. Zhang, X. Fang, D. Yan, *Inorg. Chem. Front.* **2021**, *8*, 1762–1770.
[26] J. Zhou, X. Liu, X. Xu, X. Sun, D. Wu, H. Ma, X. Ren, Q. Wei, H. Ju, *ACS Sustainable Chem. Eng.* **2021**, *9*, 13399–13405.
[27] Z. Y. Wu, M. Karamad, X. Yong, Q. Huang, D. A. Cullen, P. Zhu, C. Xia, Q. Xiao, M. Shakouri, F. Y. Chen, J. Y. T. Kim, Y. Xia, K. Heck, Y. Hu, M. S. Wong, Q. Li, I. Gates, S. Siahrostami, H. Wang, *Nat. Commun.* **2021**, *12*, 2870.
[28] C. Li, R. Xu, S. Ma, Y. Xie, K. Qu, H. Bao, W. Cai, Z. Yang, *Chem. Eng. J.* **2021**, *415*.
[29] J. Gao, B. Jiang, C. Ni, Y. Qi, Y. Zhang, N. Oturan, M. A. Oturan, *Appl. Catal. B.* **2019**, *254*, 391–402.
[30] W. Fu, X. Du, P. Su, Q. Zhang, M. Zhou, *ACS Appl. Mater. Interfaces* **2021**, *13*, 28348–28358.
[31] Y. Wang, A. Xu, Z. Wang, L. Huang, J. Li, F. Li, J. Wicks, M. Luo, D. Nam, C. Tan, Y. Ding, J. Wu, Y. Lum, C. Dinh, D. Sinton, G. Zheng, E. Sargent, *J. Am. Chem. Soc.* **2020**, *142*, 5702–5708.
[32] H. Liu, J. Park, Y. Chen, Y. Qiu, Y. Cheng, K. Srivastava, S. Gu, B. Shanks, L. Roling, W. Li, *ACS Catal.* **2021**, *11*, 8431–8442.
[33] R. Zhang, Y.-C. Zhang, L. Pan, G.-Q. Shen, N. Mahmood, Y.-H. Ma, Y. Shi, W. Jia, L. Wang, X. Zhang, W. Xu, J.-J. Zou, *ACS Catal.* **2018**, *8*, 3803–3811.
[34] Y. Rao, S. Chen, Q. Yue, Y. Kang, *ACS Catal.* **2021**, *11*, 8097–8103.
[35] S. S. Shinde, A. Sami, J.-H. Lee, *J. Mater. Chem. A.* **2015**, *3*, 12810–12819.
[36] K. Fan, Y. Ji, H. Zou, J. Zhang, B. Zhu, H. Chen, Q. Daniel, Y. Luo, J. Yu, L. Sun, *Angew. Chem. Int. Ed.* **2017**, *56*, 3289–3293.
[37] P. Wei, H. Xie, X. Zhu, R. Zhao, L. Ji, X. Tong, Y. Luo, G. Cui, Z. Wang, X. Sun, *ACS Sustainable Chem. Eng.* **2019**, *8*, 29–33.
[38] G. Wen, J. Liang, Q. Liu, T. Li, X. An, F. Zhang, A. A. Alshehri, K. A. Alzahrani, Y. Luo, Q. Kong, X. Sun, *Nano Res.* **2021**, *15*, 972–977.
[39] L. Zhang, J. Liang, Y. Wang, T. Mou, Y. Lin, L. Yue, T. Li, Q. Liu, Y. Luo, N. Li, B. Tang, Y. Liu, S. Gao, A. A. Alshehri, X. Guo, D. Ma, X. Sun, *Angew. Chem. Int. Ed.* **2021**, *60*, 25263–25268.
[40] Z. Li, Z. Ma, J. Liang, Y. Ren, T. Li, S. Xu, Q. Liu, N. Li, B. Tang, Y. Liu, S. Gao, A. A. Alshehri, D. Ma, Y. Luo, Q. Wu, X. Sun, *Mater. Today Phy.* **2022**, *22*, 100586.
[41] Y. Lin, J. Liang, H. Li, L. Zhang, T. Mou, T. Li, L. Yue, Y. Ji, Q. Liu, Y. Luo, N. Li, B. Tang, Q. Wu, M. S. Hamdy, D. Ma, X. Sun, *Mater. Today Phy.* **2022**, *22*, 100611.
[42] Z. Wu, M. Karamad, X. Yong, Q. Huang, D. Cullen, P. Zhu, C. Xia, Q. Xiao, M. Shakouri, F. Chen, J Kim, Y. Xia, K. Heck, Y. Hu, M Wong, Q. Li, I Gates, S. Siahrostami, H. Wang, *Nat. Commun.* **2021**, *12*, 2870.
[43] R. Jia, Y. Wang, C. Wang, Y. Ling, Y. Yu, B. Zhang, *ACS Catal.* **2020**, *10*, 3533–3540.
[44] Y. Guo, R. Zhang, S. Zhang, Y. Zhao, Q. Yang, Z. Huang, B. Dong, C. Zhi, *Energ. Environ* **2021**, *14*, 3938–3944.
[45] D. Reyter, G. Chamoulaud, D. Bélanger, L. Roué, *J. Electroanal. Chem.* **2006**, *596*, 13–24.
[46] Y. Zhang, Y. Zhao, Z. Chen, L. Wang, P. Wu, F. Wang, *Electrochim. Acta* **2018**, *291*, 151–160.
[47] M. Chen, J. Bi, X. Huang, T. Wang, Z. Wang, H. Hao, *Chemosphere* **2021**, *278*, 130386.
[48] Y. Yu, C. Wang, Y. Yu, Y. Wang, B. Zhang, *Sci. China Chem.* **2020**, *63*, 1469–1476.

Manuscript received: July 27, 2023
Accepted manuscript online: July 31, 2023
Version of record online: ■■, ■■

RESEARCH ARTICLE

Fe doping CoS_2 nanoarrays can effectively catalyze the formation of NH_3 from nitrate (NO_3^-) under ambient conditions. At −0.9 V (vs. RHE), the NH_3 yield rate (R_{NH3}) of Fe–CoS_2/CC is 17.8×10^{-2} mmol h^{-1} cm^{-2} with a Faraday efficiency (FE) of 88.93 %.

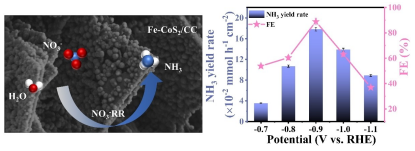

X. Lu, J. Zhou, J. Zhao, Prof. D. Wu, X. Liu, Prof. X. Ren, Prof. Q. Wei*, Prof. H. Ju*

1 – 7

Fe-Doped CoS_2 Nanoarrays: Efficient Electrocatalytic Nitrate Reduction to Ammonia under Ambient Conditions

SPACE RESERVED FOR IMAGE AND LINK

Share your work on social media! *ChemPhysChem* has added Twitter as a means to promote your article. Twitter is an online microblogging service that enables its users to send and read short messages and media, known as tweets. Please check the pre-written tweet in the galley proofs for accuracy. If you, your team, or institution have a Twitter account, please include its handle @username. Please use hashtags only for the most important keywords, such as #catalysis, #nanoparticles, or #proteindesign. The ToC picture and a link to your article will be added automatically, so the **tweet text must not exceed 250 characters**. This tweet will be posted on the journal's Twitter account (follow us @ChemPhysChem) upon publication of your article in its final form. We recommend you to re-tweet it to alert more researchers about your publication, or to point it out to your institution's social media team.

ORCID (Open Researcher and Contributor ID)

Please check that the ORCID identifiers listed below are correct. We encourage all authors to provide an ORCID identifier for each coauthor. ORCID is a registry that provides researchers with a unique digital identifier. Some funding agencies recommend or even require the inclusion of ORCID IDs in all published articles, and authors should consult their funding agency guidelines for details. Registration is easy and free; for further information, see http://orcid.org/.

Xiaoliang Lu
Jinzhi Zhou
Jinxiu Zhao
Prof. Dan Wu
Xuejing Liu
Prof. Xiang Ren http://orcid.org/0000-0002-4321-4282
Prof. Qin Wei
Prof. Huangxian Ju